International Journal of Hydrogen Energy 72 (2024) 839–849

Contents lists available at ScienceDirect

International Journal of Hydrogen Energy

journal homepage: www.elsevier.com/locate/he

Hydrogen-rich syngas derived from smouldering biomass and hydrocarbon wastes

Joshua K. Brown [a,b], Tarek L. Rashwan [c,*], Jason I. Gerhard [a,‡]

[a] Department of Civil and Environmental Engineering, The University of Western Ontario, London, Ontario, N6A 5B9, Canada
[b] Savron, 605 Boxwood Dr., Cambridge, Ontario, N3E 1A5, Canada
[c] School of Engineering and Innovation, The Open University, Milton Keynes, MK7 6AA, UK

ARTICLE INFO

Handling Editor: Umit Koylu

Keywords:
Smoldering
Hydrogen
Gasification
Syngas
Waste management
Biomass

ABSTRACT

Smouldering has recently been developed as a cost effective and energy efficient technology for challenging wastes. These systems are often used to eliminate environmental liabilities, and only minimal work has explored their use for generating useful by-products. This study addressed this research gap and demonstrated that applied smouldering systems can be tuned to favour hydrogen production. Calcium oxide and steam were added to the smouldering system, which completely treated woody biomass and coal tar, while producing hydrogen. The maximum hydrogen concentration achieved in the smouldering system was 33.7%, resulting in a net energy positive syngas. Results suggest that both heterogenous gasification and the water gas shift were key mechanisms behind hydrogen formation. These results indicate that smouldering systems can be used as a new method to sustainably produce hydrogen-rich syngas from challenging wastes.

1. Introduction

The world is currently experiencing higher energy demand than ever before with projections indicating a 50% increase in global energy usage by 2050 [1]. This increased energy demand is occurring while the world is in the midst of a climate crisis brought on by the exploitation of fossil fuels [2]. The estimated cost of climate change could be up to $23 trillion globally by 2050 [3]. Despite this, fossil fuels have accounted for approximately 80% of the global energy consumption from 2009 to 2019 [4]. New energy sources are needed to meet the surging energy demand while curtailing the use of fossil fuels.

1.1. H_2 energy and production

H_2 is recognized as a potential green fuel that could replace fossil fuels in many energy systems, either through combustion or use in fuel cells [5–8]. Since H_2 does not exist abundantly and freely in nature, it is considered a secondary source of energy or, more commonly, an energy carrier rather than an energy source. H_2 has one of the highest gravimetric energy densities, which is approximately three times greater than gasoline and natural gas. This characteristic makes it an excellent energy carrier. Therefore, H_2 can serve as a storage and/or transport medium for energy derived from primary sources (e.g., fossil fuels, biomass, renewables). Abating high-carbon emitting fuels by converting their inherent energy to H_2 is an attractive prospect in the current fight against climate change.

Beyond the energy sector, H_2 is already a valuable resource. Of the 95 million tonnes of H_2 consumed globally in 2022, approximately 33% was used to create ammonia in fertilizers, which are critical to ensuring the global food supply. Additionally, methanol production accounted for ~17%, where ~5% was used in the steel industry [9].

Despite its promise, H_2 is difficult to produce economically and sustainably [10]. Numerous technologies at varying levels of maturity exist to produce H_2, and it remains an area of active research. The methods used to produce H_2 are diverse and have been categorized into different colours based on the process, primary fuel used, and type of energy used. A brief description of the major technologies and their shortcomings is provided below.

Grey H_2 broadly describes H_2 produced from steam reforming of fossil fuels (typically steam methane reforming; SMR) or coal gasification (sometimes called black/brown H_2) with no carbon capture. These are the most mature H_2 production technologies [11,12,13], but they produce significant amounts of CO_2 and requires continuous energy inputs and catalyst replacements [14]. Despite their drawbacks, grey H_2 technologies are well-established and exhibit some of the lowest raw

* Corresponding author. School of Engineering and Innovation, The Open University, Milton Keynes, MK7 6AA, UK.
E-mail addresses: jkbrown@savronsolutions.com (J.K. Brown), tarek.rashwan@open.ac.uk (T.L. Rashwan).
‡ Deceased.

https://doi.org/10.1016/j.ijhydene.2024.05.289
Received 4 March 2024; Received in revised form 9 May 2024; Accepted 18 May 2024
Available online 3 June 2024

List of abbreviations

CCS	Carbon capture and storage
CH_4	Methane
CO	Carbon monoxide
CO_2	Carbon dioxide
CT	Coal tar
CT x2	Coal tar with double the mass concentration
CT x4	Coal tar with quadruple the mass concentration
GAC	Granular activated carbon
H_2	Hydrogen
O	Atomic oxygen
SMR	Steam methane reforming
SP	Sampling probe
TC	Thermocouple
WC	Wood chips

costs and highest H_2 yields of thermal conversion technologies [15].

Blue H_2 is from SMR with carbon capture and storage (CCS) and is an attempt to reduce carbon emissions from grey H_2 production. As such, blue H_2 is viewed as a stop-gap as newer, more environmentally friendly production methods are developed. Moreover, blue H_2 technologies can suffer from decreased process efficiencies [16] and the amount carbon capture possible has not yet been satisfactorily demonstrated at large scales [13].

The use of electrolyzers to split water to generate H_2 are typically divided into yellow, pink, and green H_2. Yellow H_2 utilizes grid electricity, pink H_2 utilizes electricity specifically from a nuclear facility, while green H_2 utilizes electricity from renewables such as wind or solar. Electrolysis can be used to generate H_2 by splitting water with an electric current and is considered a promising, clean H_2 production technology. Electrolysis, though able to create high purity H_2 with great efficiency [10,17,18], struggles to be economically viable at large scales [10]. The production costs for yellow and green H_2 are, on average, 6–8 times higher than SMR and the capital cost of an electrolysis plant can be prohibitively expensive relative to thermal conversion technologies at high capacities [14]. Ultimately, green H_2 technologies exhibit many benefits as highly sustainable methods to generate clean H_2, but they struggle to compete economically in the current market.

Gasification technologies are well-established, but it is still challenging to produce high H_2 yields from some biomass feedstocks. Gasification generates H_2 and a blend of other reduced gases – collectively referred to as syngas. Biomass gasification is a promising approach that can achieve comparable conversion efficiencies to coal gasification [14] from a variety of feedstocks with a comparatively low carbon footprints [19–21]. Despite being a robust field of research, a definitive colour has not been given to H_2 produced from biomass gasification [13].

Biomass is an abundant resource globally with an estimated 181.5 billion tonnes available [22]. Unfortunately, the diversity of biomass feedstocks results in an inconsistent fuel with a high concentration of impurities. Feedstock pre-processing can be an economic limitation, as significant energy may be needed to condition the feedstock to promote H_2-forming reactions [19] and reduce the overall process energy efficiency [14]. Regardless, tar formation is a major issue with biomass gasification, which can lead to equipment wear and tear/failures and catalyst poisoning [23]. A significant energy input is required to decompose the tar – requiring temperatures more than 1250 °C for at least 0.5 s [24].

Further technological developments that can help bridge the gap between grey and green H_2 are needed .

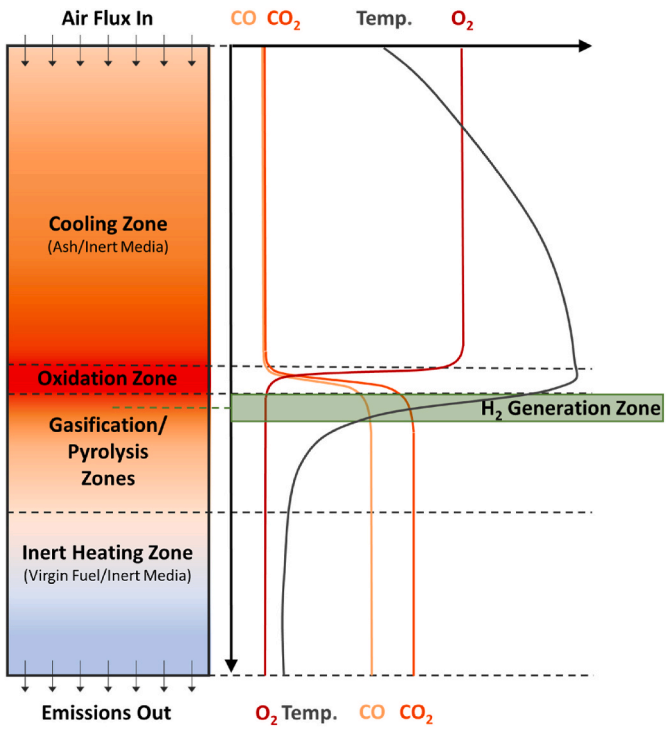

Fig. 1. Key smouldering zones - including the H_2 generation zone - with corresponding temperature and emission profiles.

1.2. Applied smouldering

Recently, smouldering has been used as a cost-effective technology for multiple applications, including contaminated soil remediation [25–28] and waste management [29–31]. Smouldering is a flameless form of combustion, driven by oxygen attacking the surface of a condensed phase fuel [25,32,33]. A benefit of smouldering is that it can be self-sustaining across a wide range of conditions after a brief ignition event. In smouldering applications, the released heat is efficiently captured by a surrounding inert matrix, thereby storing the released reaction energy and providing a preheating region for incoming oxidant gas [34]. This energy recycling makes smouldering more resistant to quenching than flaming combustion, with a thermal buffer to tolerate system perturbations [35]. Many organic wastes/feedstocks that generally cannot be treated by other thermal technologies without pre-processing (incineration, gasification, etc. due to low volatility or high moisture contents), can often be successfully treated via smouldering.

When smouldering is used as a remediation or waste management technique, the contaminant/waste is often embedded within or blended with an inert porous matrix. The inert porous media is used to provide air permeability, increased surface area for reaction, and recycle energy released exothermically [26,30,36]. Once started, the smouldering front will progress through the matrix in the direction of the air flux and completely consume the waste as fuel. A multi-decade research campaign has explored many aspects of smouldering systems that affect process performance and controllability, e.g., permeability [26,37], moisture content limitations [26,30], and waste concentrations to control peak temperatures [31].

Smouldering systems share many similarities with updraft gasifiers, due to the development of various thermal decomposition zones (e.g., preheating) preceding the reaction zone. However, applied smouldering systems routinely use large inert fractions, which are uncommon in gasifiers and affects the dynamics of these zones. As applied smouldering systems are driven by robust oxidation, some tar formed will be consumed in the oxidation zone and, therefore, applied smouldering

Table 1
Elemental analysis of primary fuels.

Fuel	Carbon (%)	Hydrogen (%)	Nitrogen (%)	Sulfur (%)	Oxygen (%)	Ash (%)
Coal Tar	80.75	5.72	1.19	0.85	10.78	0.71
Wood Chips	47.76	5.28	0.10	0.45	41.59	4.82
GAC	87.54	0.65	0.08	0.38	9.86	1.48

may not suffer the same negative effects from tar formation that can hinder gasifiers. Despite many advances in applied smouldering science, only a few studies have demonstrated the potential to produce H_2 reliably from smouldering systems [38–40]. No systemic effort has explored practical methods to promote H_2 production towards economic yields.

Fig. 1 shows a conceptual diagram illustrating the temperature and emissions profiles over the key smouldering zones, as described by Torero et al., [33], with the H_2 generation zone overlain.

The oxidation zone in applied smouldering systems is characterized by a thin region (usually a few mm or cm thick), where the oxygen and fuel are depleted and exothermic energy is released [40–42]. The heat released from oxidation is transferred forward to pyrolyze and gasify the fuel ahead. Pyrolysis and gasification reactions do not have well-defined boundaries in these systems and often compete where oxygen is depleted [40]. However, gasification reactions will likely dominate near the oxidation zone, where temperatures are hotter, while pyrolysis will dominate further from the oxidation zone, where temperatures are cooler. The narrow band preceding the oxidation zone is ideal for H_2 production. Within this band, the carbon char is super-heated (i.e., >500 °C, depending on smouldering conditions), and the emissions consists of light hydrocarbon gases and carbon oxides in an anoxic environment. These conditions are well-suited for heterogeneous and homogeneous H_2 production.

This study explores various practical strategies to promote H_2 production in applied smouldering systems from complex waste feedstocks that are typically problematic in other thermal conversion technologies (gasification, pyrolysis, etc.). An experimental suite was conducted to evaluate the effects of fuel/feedstock, porous media, CaO, and steam on H_2 production. System parameters were then adjusted to maximize H_2 yields. Further analyses were conducted to elucidate the key H_2 formation mechanisms. Altogether, this study provides the first comprehensive investigation into transforming challenging wastes into H_2 utilizing a relatively new thermal conversion technology; applied smouldering.

2. Materials and methods

2.1. Smouldering mixture preparation

Granular activated carbon (GAC) (McMaster Carr, 3190K523, 40–60 mesh), coal tar (CT) (Alfa Aesar, Catalog# 42,488), and wood chips (WC) (BRQ Fibre et Broyure Inc., Trois Rivieres, QC) were the primary fuels used in this study and their elemental analysis is shown in Table 1. Canola oil (Saporito Foods) and crumb rubber (Emterra, 10–20 mesh) were also used in select experiments (see Supplementary Material B).

Fuels were mixed with coarse grained silica sand (K & E Sand and Gravel, WP2-50A60, 8–16 mesh) in a stand mixer (KitchenAid, Professional 600TM). To achieve smouldering temperatures above 800 °C, 30 g kg^{-1} of GAC was added to all mixtures [31]. CaO has been shown to improve both steam methane reforming and gasification by scrubbing produced CO_2 [43–46]. As CO_2 is removed from the reaction, the thermodynamic equilibrium shifts to favour the production of other products, including H_2. CaO has also been shown to have catalytic properties that promote H_2 formation [47]. CaO was first mixed into the coal tar to minimize the formation of calcium hydroxide ($Ca(OH)_2$). By embedding the CaO in the coal tar solution, the steam was prevented from contacting the CaO until the coal tar underwent degradation via pyrolysis/combustion when the temperatures were above the dehydration temperature of calcium hydroxide (i.e., > 400 °C) [48,49]. Sand was the primary inert porous medium used in this study for Tests 1–8. Tests 9–11 used alumina (InTerra, aSORB Activated Alumina, 1.5–2 mm) as the inert porous medium to explore its effect on H_2 production. Test 12 used wood chips as a smoulderable porous medium to create a fully smoulderable mixture. To maintain consistent fuel loading, the same mass of coal tar, GAC, and CaO were added in all tests, regardless of the porous media used. Further details on all tests are included in Table 2.

2.2. Experimental apparatus

All experiments were conducted in a purpose-built smouldering reactor, similar to the reactors used by others in the literature [39,50,51]. A cross-section of this reactor is shown in Fig. 2.

The 11 cm diameter, 94 cm tall stainless-steel reactor was wrapped in

Table 2
Experimental conditions for smouldering experimental suite.

Test	Bulking Matrix	Organic Fuel	Fuel Conc (g kg^{-1})	GAC Conc (g kg^{-1})	GAC Mass (g)	Coal Tar Mass (g)	Wood Chips Mass (g)	Total Fuel Carbon (g)	CaO Ratio (mass)	Air Flux (cm s^{-1}) ± 1%	Steam Rate (g min^{-1})± 2g	Steam/C Ratio (mol mol^{-1})
1	Sand	GAC	0	30	189.2	–	–	165.6	–	2.5	9.95	5.3
2	Sand	Coal Tar	30	30	173.9	174.3	–	293.0	–	2.5	9.95	3.8
3	Sand	Coal Tar	30	30	164.3	164.0	–	276.3	–	2.5	18.46	6.9
4	Sand	Coal Tar	30	30	162.9	163.0	–	274.2	1:1 CT: CaO	2.5	18.5	7.3
5	Sand	Coal Tar	60	30	151.3	302.4	–	376.6	2:1 CT: CaO	2.5	21.3	6.1
6	Sand	Coal Tar	120	30	156.4	625.3	–	641.8	2:1 CT: CaO	2.5	18.8	6.6
7	Sand	Coal Tar	120	30	156.9	626.8	–	643.5	2:1 CT: CaO	5.0	23.0	3.4
8	Sand	Wood Chips	125	75	213.3	–	355.2	356.4	2:1 WC: CaO	5.0	20.5	3.1
9	Alumina	Coal Tar	200	50	151.1	603.4	–	619.5	2:1 CT: CaO	5.0	13.0	2.0
10	Alumina	Coal Tar	200	50	148.4	593.9	–	609.5	2:1 CT: CaO	5.0	21.6	3.2
11	Alumina	Wood Chips	220	132	214.6	–	357.2	358.5	2:1 WC: CaO	5.0	19.6	2.4
12	Wood Chips	Wood Chips & Coal Tar	–	30	155.5	626.8	518.3	889.8	2:1 CT: CaO	5.0	21.1	2.1

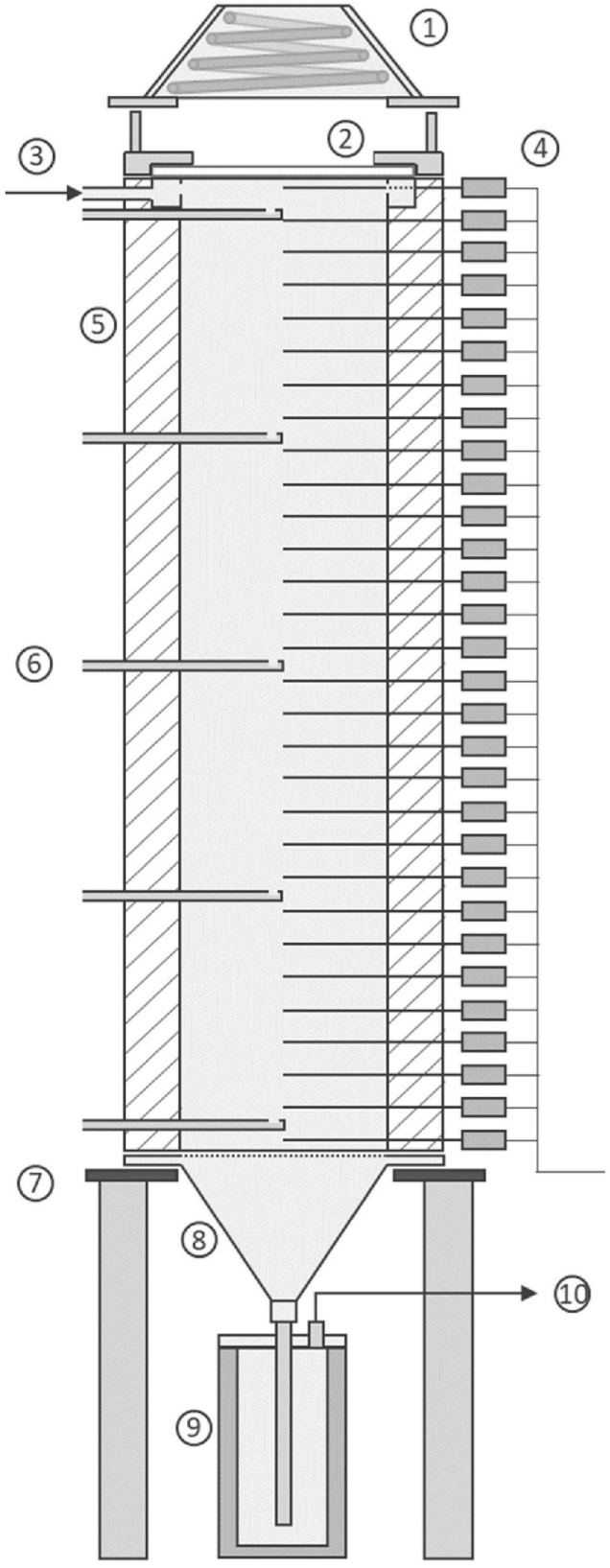

Fig. 2. Radiative Ignition Smouldering Reactor – 1. Cone heater, 2. Quartz window, 3. Air inlet to circumferential air plenum, 4. Thermocouples (30 TCs with 3 cm spacing), 5. Insulation and stainless-steel jacket, 6. Sampling probes (5 SPs with 21 cm spacing), 7. Reactor stand, 8. Reducing cone with perforated flange face, 9. Knock-out with chilled water jacket, 10. Emissions outlet.

two layers of insulation (Firwin Plus, 160 kg m^{-3}, 0.22 W m^{-1} K^{-1} at 1000 °C), where the first and second layers were 0.5 and 5 cm thick, respectively. This reactor diameter ensured that the chemistry along the centerline was not strongly influenced by heat losses [50,52]. The height allowed for the smouldering reactions to reach steady-state conditions. In this study, steady-state smouldering conditions were characterized as when the peak temperatures, emission concentrations, and smouldering velocities became constant over time. In many laboratory-scale applied smouldering systems, these steady-state conditions are achieved after the smouldering front propagates ~0.1 m [52,53]. The reactor was sealed on the bottom end by a reducing funnel flange topped with a perforated plate covered in a 100-mesh screen to support the smouldering bed. The top of the reactor was sealed with a 127 mm diameter x 6.35 mm thick optical quartz window (Esco Optics, P650250), held in place by a custom flange. Graphite gaskets were used between all flange connections. A radiative cone heater (FTT, 240V/5 kW, Part# U135) offset 5 cm from the quartz window supplied a relatively even heat flux across the top of the smouldering bed material during pre-heating.

The reactor was instrumented to provide high-resolution temperature data. Centerline temperatures were measured by K-type thermocouples (TCs) (Omega, KQIN-18U-6) at 3 cm intervals along the reactor length. All TC data was recorded at 2-s intervals on a datalogger (Agilent, 34980A).

All smouldering experiments were conducted in a top-down orientation (i.e., smouldering would be initiated at the top of the reactor and progress downwards). 43 cm of clean filter sand was placed in the bottom of the reactor on the perforated plate up to TC17. The waste mixture was then packed on top of the filter sand in small lifts until flush with the top flange and then sealed under the quartz window (i.e., between TCs1-16, with a total mixture length of 51 cm). The cone heater was turned on to pre-heat the mixture to ignition. Once 450 °C was measured at the first TC (i.e., TC1 ~0.25 cm into the bed) after 20–30 min, air was introduced to ignite smouldering.

Injected air was moderated via a mass flow controller (Omega, FMA5400/5500 Series) into the reactor through four radial wall ports located immediately below the quartz window flange (Fig. 2). Experiments were conducted at a Darcy flux of either 2.5 or 5 cm s^{-1}. Steam was added by passing the air line through the headspace of a custom-built, 4 L steam generator prior to entering the reactor. The rate of steam generation was controlled up to a maximum rate of 23 g min^{-1} by adjusting the power delivered by two resistance heaters (Watlow Ltd., 120V/450W) with a 120V AC, single phase power supply (STACO Energy products). The variac power control only allowed for coarse adjustments, which meant the steam rate exhibited some inherent variability between tests. The steam generator was seated on a mass balance (AccuWeigh, PPC-200W) and the transient weight loss was recorded to determine the steam generation rate for each experiment.

Once the smouldering front became self-sustaining (i.e., when the smouldering reactions generated sufficient rate of exothermicity to overwhelm local heat loss rates), the heater was turned off and the smouldering front proceeded downwards, supported only by the air supply.

2.3. Gas sampling and analysis

In-situ gas samples were taken from the bottom two of the five multi-purpose sampling probes (i.e., SP4 and SP5). Emissions were drawn through a knock-out canister and desiccant tower (Drierite, 26,800) chilling conditioning drawer (Universal Analyzers Inc., SCD) from SP5 (86.5 cm) to dry the gas stream. These dry emissions were then analyzed continuously for CO_2, CO, and O_2 concentrations (MGA3000 Multi-Gas Analyzer). The emissions concentrations were recorded on the same time interval and data logger as the temperature measurements (Agilent, 34980A).

Table 3
Key emissions and smouldering results.

Test	Purpose	Bulking Matrix	Organic Fuel	Total C (g)	Air Flux (cm s^{-1}) ± 1%	Steam Rate (g min^{-1}) ± 2g	Steam/C Ratio (mol mol^{-1})	Average Front Velocity (cm min^{-1})	Average Peak Temp (°C)	Steady-State CO_2 Conc (%) ± 0.2%	Steady-State CO Conc (%) ± 0.2%	Steady-State H_2 Conc (%)[a]	Steady-State CH_4 Conc (%)[a]	Total Syngas E (kJ)
1	Baseline with GAC amendment used in all subsequent tests.	Sand	GAC	165.6	2.5	10.0	5.3	0.45	823.5	13.6	5.5	0.7	–	1131
2	Addition of coal tar waste fuel with volatile component.	Sand	Coal Tar	293.0	2.5	10.0	3.8	0.41	1055.9	14.5	9.8	2.5	–	2570
3	Increasing the steam rate by ~2x (similar steam rate used in all subsequent tests, except Test 9).	Sand	Coal Tar	276.3	2.5	18.5	6.9	0.50	1011.5	13.9	9.8	6.2	–	2427
4	Adding CaO to the matrix (included in all subsequent tests).	Sand	Coal Tar	274.2	2.5	18.5	7.3	0.55	1059.7	19.1	9.8	10.2	–	3626
5	Increasing coal tar concentration ~2x.	Sand	Coal Tar	376.6	2.5	21.3	6.1	0.53	1017.2	18.9	8.6	12.0	–	4184
6	Increasing coal tar concentration ~4x (this mass loading was used in all subsequent coal tar tests).	Sand	Coal Tar	641.8	2.5	18.8	6.6	0.45	1010.9	18.1	5.6	14.3	–	4267
7	Increasing the air flux ~2x (this air flux was used in all subsequent tests).	Sand	Coal Tar	643.5	5.0	23.0	3.4	0.94	1213.5	17.7	9.1	13.8	–	4906
8	Substituting wood chips for coal tar as the organic fuel.	Sand	Wood Chips	356.4	5.0	20.5	3.1	0.99	931.3	21.2	5.2	10.3	0.60	3043
9	Repeat of Test 7 substituting alumina for sand as the bulking matrix. Steam rate decreased to a steam/C ratio of ~2.	Alumina	Coal Tar	619.5	5.0	13.0	2.0	1.47	1235.5	15.2	9.8	12.7	0.07	3919
10	Repeat of Test 9 with alumina matrix but with a steam/C ratio of ~3 (similar steam/C ratio as Test 7).	Alumina	Coal Tar	609.5	5.0	21.6	3.2	1.27	1144.8	15.6	9.1	17.4	0.10	4915
11	Repeat of Test 8, except substituted alumina for sand as the bulking matrix.	Alumina	Wood Chips	358.5	5.0	19.6	2.4	2.38	932.7	20.7	8.7	12.6	0.59	4038
12	Using wood chips as the bulking matrix with the same coal tar mass loading used previously.	Wood Chips	Wood Chips & Coal Tar	889.8	5.0	21.1	2.1	–	999.1	22.4	6.2	26.2	0.32	11,392

[a] Relative standard deviation of H_2 and CH_4 for each test included in Supplementary Material B.

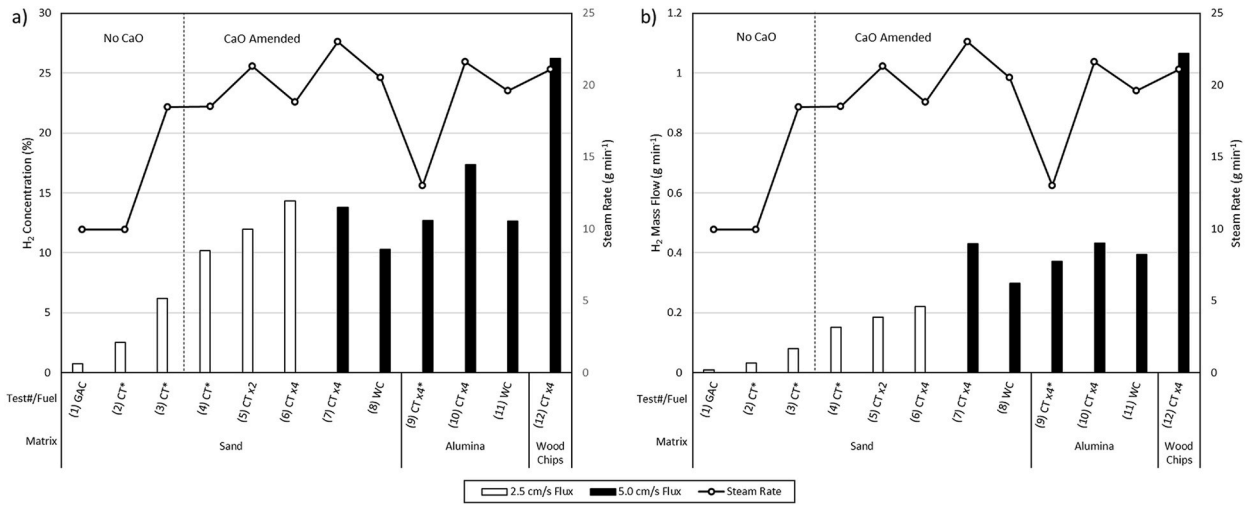

Fig. 3. Figure 3a) Steady-state H_2 concentrations and injected steam rate. 3b) Steady-state H_2 mass flow and injected steam rate. GAC: Granular Activated Carbon, CT: Coal Tar, WC: Wood Chips, x2 and x4: doubled and quadrupled concentrations, respectively. Experiments with asterisks indicate CO measurement was above the detectable range of the instrument (vol. 10%).

Emissions were also collected for Gas Chromatography – Thermal Conductivity Detector (GC-TCD) analysis from SP4 (i.e., 65.5 cm) at early-, mid-, and late-times, i.e., when the TC2, TC8, and TC14 reached peak temperatures, respectively. The mid-time gas results are presented in the main manuscript as they were the most representative of the steady-state conditions. That is, the mid-time results were least affected by initial- and end-effects associated with smouldering ignition and completion, respectively. The early- and late-time results and relative standard deviation can be seen in the Supplementary Material B. SP4 was connected to a 5L Tedlar bag (Restek, Catalog# 22,052), which was opened during the sampling period and filled from the positive pressure in the reactor. A custom-built vacuum chamber was used to transfer the contents of the Tedlar bag grab samples into GC vials for GC-TCD analysis. GC-TCD analysis was used to quantify the H_2 and CH_4 concentrations from grab samples (Table 3, Supplementary Material A). The syngas energy was estimated from the enthalpy of combustion for the emission mass flows of H_2, CO, and CH_4. As discussed previously, the H_2 and CH_4 concentrations consisted of three samples taken over the duration of the test and therefore exhibited a much lower resolution in time than CO measurements, which were logged every two seconds. Any additional combustible products were also missed by this analysis, which implies that the calculated syngas energy estimate is conservatively low.

3. Results and discussion

Results from the twelve tests are summarized in Table 3. The results show that the parameters varied in this work increased the steady-state H_2 production from 0.7% up to 26.2%. The effects of each amendment and the relevant mechanisms are discussed in Section 3.3.

3.1. Process amendment results

The effect of fuel type/loading, porous media type, CaO addition, and steam injection were all explored to understand their influences on H_2 production. The steady-state H_2 concentrations and H_2 production rates are presented in Fig. 3a and b, respectively.

A GAC/steam system was used as the base case (i.e., Test 1). Since GAC does not produce H_2 when it is smouldered without steam, it was a conservative fuel amendment that could be added to increase combustion temperatures without adding a significant amount of molecular hydrogen to the system. Note that 30 g kg^{-1} of GAC/sand was added to all experiments to ensure the peak smouldering temperatures exceeded 800 °C and 9.95 g min^{-1} of steam was the minimum rate explored in this work. These operational conditions yielded a steady-state H_2 concentration of 0.7% (Fig. 3, Table 3).

Additional experiments were conducted to explore H_2 production from smouldering unamended, virgin fuels including GAC, coal tar, crumb rubber, and wood chips (see Supplementary Material). The H_2 concentrations emitted during smouldering were all very small since H_2 is not a thermodynamically favourable product of combustion. The minimal H_2 production during conventional smouldering would be due to pyrolysis ahead of the smouldering combustion reactions, where most emissions are generated [33]. GAC, which contains virtually no molecular hydrogen, did not produce any H_2. Wood chips produced the greatest quantity of H_2, followed by coal tar and crumb rubber. This trend indicates that there is a general negative correlation between the degree of fuel processing and H_2 production.

Coal tar was added as an additional fuel with a volatile fraction (Test 2) that increased the steady-state H_2 concentration to 2.5%. When the steam rate was approximately doubled from Test 2 to Test 3, the H_2 concentration increased further to 6.2% in Test 3. Both amendments demonstrated the positive effects of adding additional reactants to the system. Increasing the fuel content was further explored in Tests 5 and 6 when the coal tar concentration was doubled and then quadrupled relative to Test 3, resulting in H_2 concentrations of 12.0% (Test 5) and 14.3% (Test 6).

A 1:1 mass ratio of CaO to coal tar was added to Test 4, resulting in a 65% increase in H_2 concentration from Test 3 (i.e., without CaO). Increasing the fuel to CaO ratio to 2:1 was found to improve H_2 production (Supplementary Material); therefore, the 2:1 fuel:CaO ratio was used for the remainder of the experimental suite.

The air flux was doubled from Tests 6 to 7, which did not have an affect on the total H_2 produced but did result in a more efficient H_2 production (see further discussion in Section 3.2.1).

Unlike the experiments with sand (i.e., Tests 1–8), which required that the smouldering front travelled ~0.1 m to reach steady-state H_2 emissions, the experiments with alumina (i.e., Tests 9–10) typically had higher H_2 concentrations throughout the entire test length and reached steady-state concentrations quickly (i.e., their early-time and mid-time H_2 concentrations were very similar – see Supplementary Material). In other words, the thermal properties of alumina (particularly, the low bulk density) fostered a rapid transition to steady-state conditions with faster propagation velocities, more energetic emissions, and overall improved H_2 production.

Less H_2 was produced when wood chips were used as the fuel source

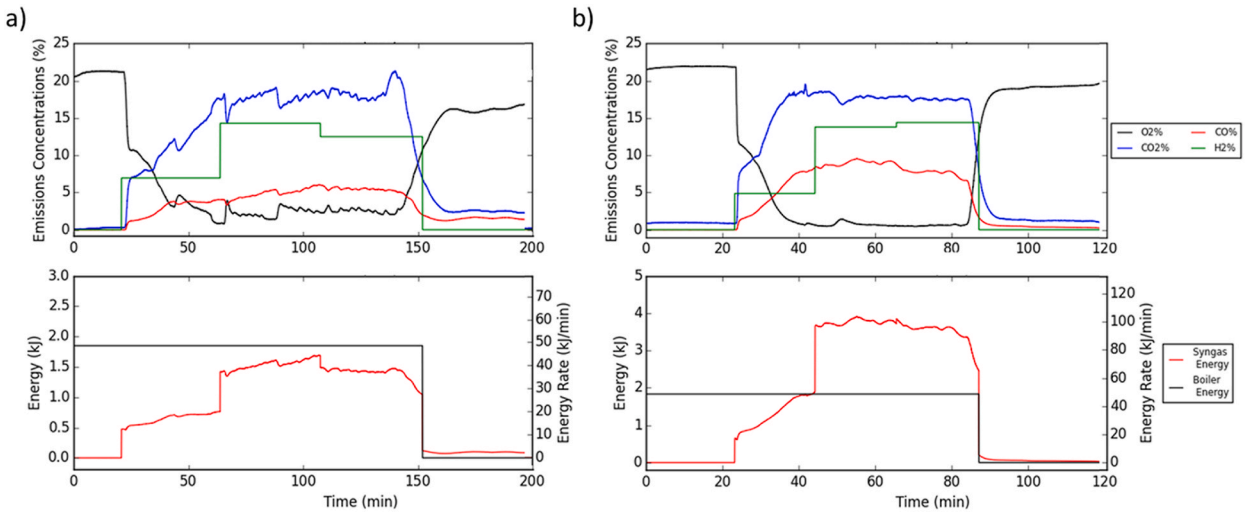

Fig. 4. Emissions species' concentrations and syngas energies during smouldering compared to boiler input energies in a) Test 6 (2.5 cm s^{-1} air flux) and b) Test 7 (5.0 cm s^{-1} air flux).

at the same mass concentration as coal tar (i.e., in Tests 8 and 11, respectively). This decrease is because the wood chips had significantly lower carbon content than the coal tar. Elemental analysis found the wood chips had a carbon content of 47.76% while coal tar's carbon content was 80.75% (Table 1), which implies that less carbon fuel was available to participate in H_2 formation. When compared on a carbon mass basis (i.e., Tests 5 vs. 8) wood chips and coal tar appear to behave similarly as a fuel for H_2 production in smouldering systems. As with coal tar, H_2 production increased when alumina was used alongside wood chips, compared to tests with sand (i.e., see Tests 8 and 11, respectively).

H_2 production was maximized when wood chips were used as the bulk media and mixed with the coal tar fuel mixture (Test 12). The steady-state H_2 concentration was 26.2% with a peak concentration of 33.7%. This improved the steady-state H_2 concentration by 50.9% compared to the second-best producing experiment (i.e., Test 10). The reasons governing this high H_2 production rate are discussed in Section 3.3.2.

3.2. Key sensitivities

3.2.1. Air flux

An important difference between the H_2 concentration and the H_2 mass production rate can be seen from Test 7 results, when the air flux was doubled relative to Tests 1–6. In Fig. 3, this change in air flux has virtually no effect on the H_2 concentration between Tests 6 and 7, but it doubled the mass production rate between these tests. This trend is because the smouldering velocity and, therefore, the global process reaction rate is linearly related to the air flux [36]. The amount of H_2 produced was therefore doubled when the air flux was doubled. This trend should persist across air fluxes until excess oxygen is supplied, which would effectively lead to oxygen leakage beyond the oxidation front that would deteriorate the H_2 generation zone in Fig. 1. The emissions species' concentrations and syngas energies for Tests 6 and 7 are shown in Fig. 4, which illustrates the energy efficiency sensitivity to air flux.

The increase in energy production rate seen in Test 7 (Fig. 4b) was substantial enough that the overall system becomes net energy positive, i.e., with respect to the energy required to drive steam generator during steady-state smouldering. Since steam needs to be created to produce meaningful H_2 fractions, the energy available from the product syngas should ideally offset the energy required for steam production. Note that the heater energy for ignition is a relatively short-duration event over the course of smouldering, where the overall energy contribution is increasingly negligible in sufficiently long smouldering systems [28,29,54,55] or if a continuously fed smouldering reactor was used [56].

3.2.2. Sensitivities to feedstock, carbon, and steam

The primary mechanisms that produce H_2 involve reactions between steam and carbon. The efficiency of converting carbon and steam in the

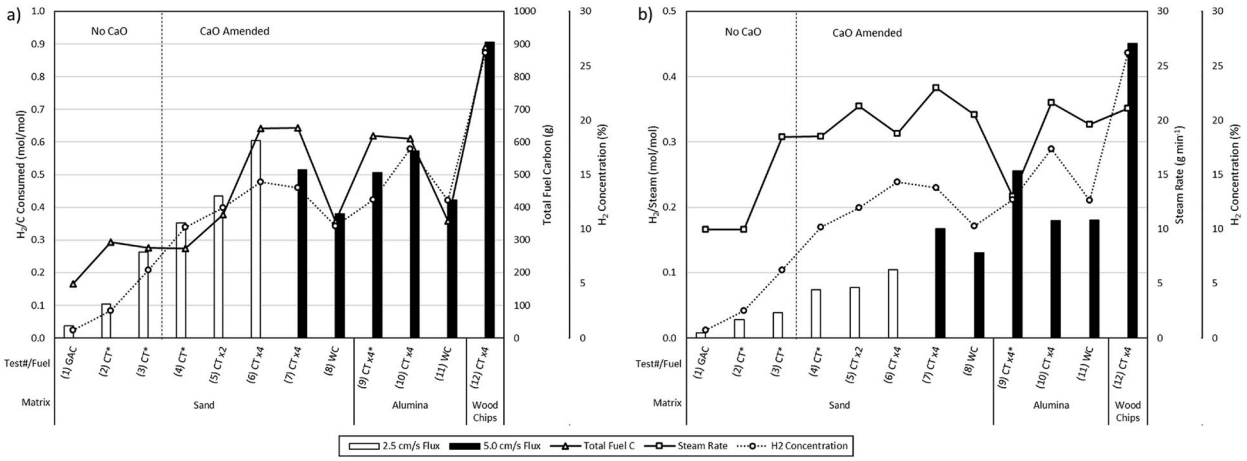

Fig. 5. H_2 production efficiency with respect to: a) carbon consumed and b) steam used. GAC: Granular Activated Carbon, CT: Coal Tar, WC: Wood Chips, x2 and x4: doubled and quadrupled concentrations, respectively. Experiments with asterisks indicate CO measurement was above the detectable range of the instrument (vol. 10%).

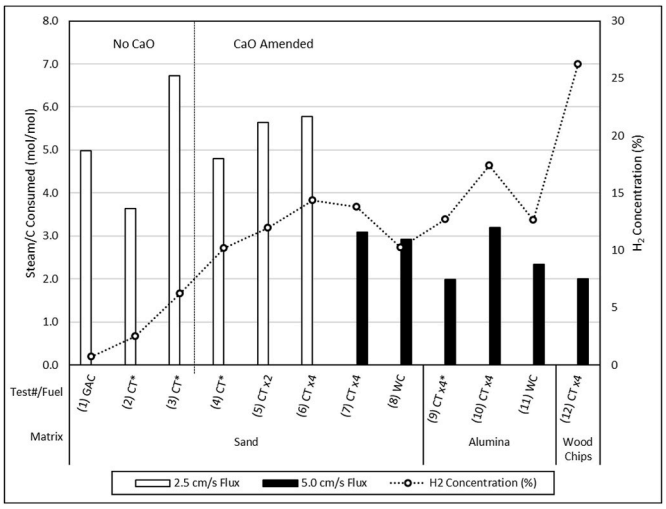

Fig. 6. Steam to carbon ratios. GAC: Granular Activated Carbon, CT: Coal Tar, WC: Wood Chips, x2 and x4: doubled and quadrupled concentrations, respectively. Experiments with asterisks indicate CO measurement was above the detectable range of the instrument (vol. 10%).

system to H_2 is explored in Fig. 5. The carbon consumed was derived from the CO_2, CO, and CH_4 emissions instead of the loaded fuel mass. Upon excavating the reactors, it was evident some of the liquid fuel mobilized out of the reaction zone, as the porous media was initially near fully saturated. This mobilization is common in smouldering systems with organic liquid wastes [57]. As such, the carbonaceous gases more accurately reflected the amount of carbon participating in smouldering and H_2 formation.

The H_2 production sensitivity to carbon can be seen across many experiments. For example, compared to Test 1 (i.e., without coal tar), the addition of coal tar (i.e., in Test 2) provided an additional volatile carbon fuel that could participate in homogeneous reactions – compared to GAC alone in Test 1, which is largely non-volatile carbon [37]. More broadly, these homogeneous volatile carbon reactions in all tests with supplemental fuels (i.e., coal tar, wood chips in Tests 2–12) improved the H_2 production compared to Test 1 (i.e., with only GAC). The H_2 production with respect to carbon (i.e., in Fig. 5a) improved with each amendment until the matrix became fully saturated with coal tar (i.e., in Test 6). A similar increase in H_2 production was observed when the steam rate was doubled (i.e., from Tests 2 to 3), which also provided more reactants for the H_2-forming reactions. An increase in efficiency was again achieved when the CaO catalyst was added to the system. Doubling the fuel (i.e., in Test 5) and then quadrupling the fuel (i.e., in Test 6) provided more carbon to react, which led to increased H_2 production.

The H_2 production sensitivity with respect to steam followed similar trends with respect to carbon for the amendments explored in Tests 1–6, but had an opposite effect when the air flux was doubled in Test 7 relative to Test 6. That is, in Tests 6 and 7, the H_2-production efficiency (*i*) slightly decreased with respect to carbon, but (*ii*) increased with respect to steam. Reasons governing the (*i*) carbon and (*ii*) steam sensitivities are detailed below.

(i) The reduced carbon efficiency may be due to increased O_2 in the system, which competed with the steam as a reactant with carbon. The carbon oxidation reactions are thermodynamically favourable and therefore additional O_2 produced more CO_2 and CO, not H_2. Indeed, when the air flux was increased from Tests 6 to 7, the average smouldering temperature also increased. This trend indicates that more energy was generated and more carbon underwent exothermic oxidation. In essence, the higher air flux reduced the amount of fixed carbon available for gasification reactions.

(ii) Conversely, since the global reaction progressed faster due to the increased air flux, less steam was used to produce the same quantity of H_2, which therefore improved H_2 production efficiency with respect to steam. The effects from reduced steam consumption were most evident in Test 9 where the steam rate was 60% of the previous Tests 3–8 and subsequent Tests 10–12. The steam efficiency was high in Test 9; however, the cost of this efficiency is evident in Fig. 3. That is, the H_2 production rate and the total H_2 mass in Test 9 were both reduced compared to Tests 7 and 10, which kept the other variables constant, i.e., fuel, air flux, and CaO. Despite the increased efficiency with respect to steam, H_2 production became steam-limited during Test 9, which reduced the overall H_2 yield. In other words, with constant fuel carbon, increased steam would increase the H_2 production with decreasing efficiency until it asymptotically reached a maximum H_2 production rate.

Carbon and steam are the two major reactants in H_2 production. They must be present in adequate quantities, otherwise the process will become either carbon- or steam-limited. Fig. 6 compares the molar ratio of steam to carbon consumed by the process.

Fig. 6 shows that the increasing H_2 production seen in Tests 1–6 was insensitive to the steam/carbon balance. This insensitivity indicates that there was excess steam in the system during Tests 1–6 and that the increasing H_2 production was a function of the other amendments and variables changed during these tests (Table 3). When the air flux was increased in Test 7 relative to Tests 1–6, the steam/carbon ratio decreased from an average of 5.8 to 3.1, respectively. The differences from Tests 1–6 to 7 marked a divergence in carbon and steam efficiencies, but had virtually no effect on the total H_2 production (see Fig. 5). Evidently, a steam/carbon ratio of 3 will not negatively impact the reaction and a higher quantity of steam will not promote additional H_2 production.

Subsequently, Test 9 reduced the amount of steam injected to a steam/carbon ratio just below 2.0. This ratio resulted in an overall reduction in H_2 production relative to similar tests with coal tar fuel (Tests 7 and 10). Specifically, Test 10 had the same experimental conditions as Test 9, except Test 10 used a steam/carbon ratio of 3.2 (Table 2) and increased the H_2 concentration to 17.4% from 12.7% in Test 9. These results suggest that the steam/carbon ratio should be maintained between 2 and 3 to foster H_2 production in applied smouldering systems. Lower ratios will result in a steam-limited system, which would throttle H_2 production. However, higher ratios will have diminishing gains.

The smoulderable matrix (i.e., wood chip matrix with coal tar fuel) in Test 12 fostered a significantly higher fuel loading, which increased the fuel carbon content in the reactor by 41% from Test 10 and ensured all steam would contact organic material rather than inert media. Indeed, as seen in Fig. 5, when wood chips were used as the bulk matrix, the H_2 production was the most efficient with respect to both carbon and steam compared to all other tests with inert media. Interestingly, the increased fuel in the system coupled with operating at the steam generator's upper limit, reduced the steam/carbon ratio down to 2.0, which approached steam-limited conditions (i.e., as informed by the results from Test 9). Steam gasification studies have found that the optimal steam/biomass mass ratio for H_2 production was between 1 and 1.5, with decreasing yields at higher ratios [58,59]. The steam/biomass mass ratio for Test 12 was 0.93, which suggests it was below the optimum ratio.

Overall, the results provide an operational roadmap for H_2 production in smouldering systems. It was found that increasing the fuel loading with co-mingled wastes, while maintaining a steam/carbon ratio between 2 and 3, created the optimal conditions to favour efficient and abundant H_2 production.

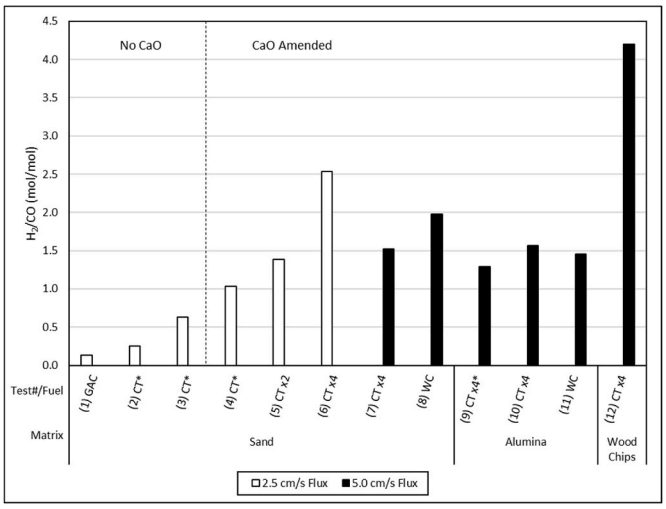

Fig. 7. Ratio of H_2 to CO generated from the reaction. GAC: Granular Activated Carbon, CT: Coal Tar, WC: Wood Chips, x2 and x4: doubled and quadrupled concentrations, respectively. Experiments with asterisks indicate CO measurement was above the detectable range of the instrument (vol. 10%).

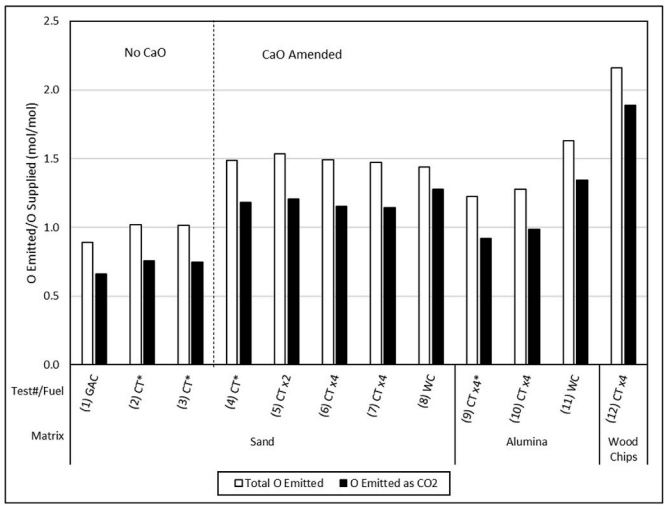

Fig. 8. Ratio of the molar quantity of the total oxygen emitted from the reaction and the oxygen emitted as CO_2 compared to the molar quantity of oxygen supplied as air to fuel to smouldering process. GAC: Granular Activated Carbon, CT: Coal Tar, WC: Wood Chip x2 and x4: doubled and quadrupled concentrations, respectively. Experiments with asterisks indicate CO measurement was above the detectable range of the instrument (vol. 10%).

3.3. Mechanisms governing H_2 production

3.3.1. Heterogeneous gasification

Heterogeneous gasification can occur just downstream of oxidation reactions where fuels have been reduced to carbon-rich char and have been heated to several hundred degrees Celsius, as shown in Fig. 1. Steam can heterogeneously react with the char in the presence of CaO and an absence of O_2, which could be fully consumed by the oxidation reactions. Solid, non-volatile GAC was used as the lone fuel source in Test 1 and produced a small amount of H_2. Heterogeneous gasification was the only mechanism available to produce H_2 in this test, which demonstrates that gasification is one of the reaction mechanisms. The gasification reaction in Eq. (1) produces equal molar parts H_2 and CO.

$$C + H_2O \rightarrow H_2 + CO \left(+131 \frac{kJ}{mol} \right) \quad (1)$$

It is therefore possible to compare the molar ratio of H_2 to CO to determine if gasification alone is responsible for the H_2 production or if other mechanisms need to be considered. Fig. 7 plots the molar ratio of H_2 to CO.

The molar ratio of H_2 to CO is greater than 1 for most tests, which indicates that gasification is not the sole mechanism. This observation is further reinforced as the CO values were inflated because smouldering also produced CO as a combustion by-product, and therefore cannot be separated from the CO produced from gasification.

In Test 2, when coal tar was used in addition to GAC, the H_2 concentration increased. A key difference between coal tar and GAC is that coal tar releases volatile carbon species during pyrolysis, which can react homogeneously with steam, and therefore foster more H_2 production than from gasification alone. This finding agrees with previous work that found more volatile fuels increased H_2 yield in steam gasification [60]. Note that Tests 1–3 fostered relatively intense oxidation reactions, which led to high CO production and low H_2/CO ratios below 1. These low ratios are not indicative that only gasification occurred. It is expected that, in all systems where volatile hydrocarbons were released, homogeneous H_2 production reactions participated as well. The exact proportion of H_2 from only heterogenous gasification cannot be determined here, but heterogeneous gasification alone does not explain the quantity of H_2 produced.

3.3.2. Homogeneous reactions

In the smouldering system, the heat transfer ahead of the oxidation front was contained to a very thin region in space [33], which resulted in the gasification and pyrolysis zones overlapping – as shown in Fig. 1. Gaseous carbon species were therefore produced near the oxidation reaction front in an anoxic region, which likely allowed them to react homogenously with steam to drive steam reformation. CO was also present in this region – both from combustion and gasification reactions. The CO could therefore undergo a water-gas shift when interacting with steam in this zone.

Steam reforming occurs when gaseous hydrocarbons react with steam following Eq (2):

$$C_xH_y + zH_2O \rightarrow \left(x + \frac{y}{2}\right)H_2 + zCO \quad (2)$$

Steam reformation can potentially produce H_2 at a ratio greater than 1 with respect to CO and could therefore have contributed to the extra H_2 observed in Fig. 7.

The water-gas shift reaction consumes CO to produce H_2 and CO_2 following Eq (3).

$$CO + H_2O \rightarrow CO_2 + H_2 \left(-41 \frac{kJ}{mol} \right) \quad (3)$$

The water-gas sift increases the ratio of H_2 to CO and could also account for the excess H_2 from Fig. 7. The participation of this reaction is confirmed by comparing the molar quantities of atomic oxygen (O) supplied to the amount emitted as CO_2 since oxidation reactions and the water-gas shift are the predominant pathways to create CO_2. Supplied air feeds the oxidation reactions and, in the event of complete combustion, the ratio of O as CO_2 emitted to O supplied does not exceed 1. Steam supplies more molecular oxygen and, when it undergoes the water-gas shift reaction, produces more CO_2. Fig. 8 shows the ratio of O emitted to O supplied.

The white bars show the total O emitted (as CO, CO_2, and O_2) vs the O supplied, while the black bars show specifically the ratio of O emitted as CO_2 to O supplied. In most tests, the ratio of CO_2 emitted to O supplied is greater than 1, which indicates the water-gas shift reaction occurred.

It is likely that a small fraction of CO_2 was produced from the

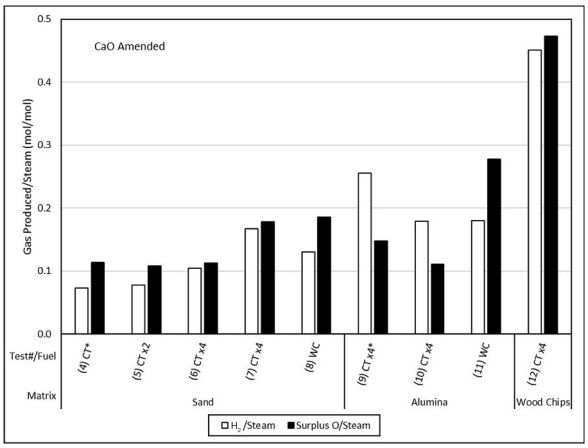

Fig. 9. Molar comparison of the excess oxygen and H_2 emitted from the reaction to the steam supplied. GAC: Granular Activated Carbon, CT: Coal Tar, WC: Wood Chips, x2 and x4: doubled and quadrupled concentrations, respectively. Experiments with asterisks indicate CO measurement was above the detectable range of the instrument (vol. 10%).

pyrolysis of coal tar and/or wood chips. The elemental analysis found that coal tar and wood chips had oxygen contents of 10.78% and 41.59%, respectively (Table 1), and a small portion of this molecular oxygen does emit as CO_2 during pyrolysis [33]. The oxygen balance was compared to the H_2 to steam ratio in Fig. 5b. For steam (H_2O) to form H_2, the molecule must split to produce equal molar amounts of H_2 and O. Therefore, the surplus O (i.e., in the emissions as CO, CO_2, and O_2 beyond what was supplied by air) to steam ratio should match the H_2 to steam ratio. Fig. 9 adds the oxygen ratio to Fig. 5b (excluding uncatalyzed tests) for comparison.

There is good agreement between the H_2 and O ratios, which provides good confidence in the mass balance and a further line of evidence that steam reformation participated in H_2 production. The oxygen ratio is higher than H_2 in most tests, likely due to the extra CO and CO_2 released from the pyrolysis of coal tar and/or wood chips. Interestingly, when alumina was used as the inert media with the coal tar (Tests 9 and 10), the H_2/steam ratio was dominant, possibly indicating a favourable matrix effect. That is, the thermophysical properties of alumina facilitated faster smouldering with improved H_2 production reactions, relative to sand.

This analysis of the reaction mechanisms indicate that heterogenous gasification cannot solely account for the yield of H_2; therefore, homogenous reactions must have also contributed. Molar ratios of oxygen and steam identified the presence of the water-gas shift. These ratios also suggested an alumina matrix promoted greater H_2 production relative to sand, which was confirmed previously with higher H_2 concentrations in Section 3.1.

4. Conclusions

Applied smouldering has been demonstrated to be a novel method to generate syngas from challenging wastes with significant H_2 concentrations – up to 33.7%. This study provided the first systematic effort exploring H_2 production across various, easy to implement modifications. This process relied on the formation of a 'H_2 generation zone', which was supported with a mineral catalyst (here: CaO) and steam injection. Results showed that the system could be tuned to produce H_2, while completely removing waste tars and biomass from the remaining ash. Moreover, the theoretical syngas energy generated was net-energy positive relative to the energy required for steam generation.

Increasing the fuel loading (i.e., carbon content) and steam both increased H_2 production, but with decreasing efficiencies. The optimum molar steam/carbon ratio appeared to be between 2 and 3. This study also identified that heterogeneous gasification, the water-gas shift, and steam reforming likely all contributed to H_2 production. Altogether, this study provides strong experimental evidence that applied smouldering systems can be tuned to foster robust H_2 production from challenging wastes.

Funding

Funding was provided by the Ontario Ministry of Research, Innovation, and Science; the Natural Sciences and Engineering Research Council of Canada (Grant Nos. CREATE 449311-14, RGPIN 2018–06464, and RGPAS-2018-522,602); the Royal Society (RG\R2 \232528), and The Open University through Engineering & Innovation Research Funding, Higher Education Innovation Funding Knowledge Transfer Vouchers, and the Open Societal Challenges Programme in support of the SPLICE challenge.

CRediT authorship contribution statement

Joshua K. Brown: Conceptualization, Data curation, Formal analysis, Investigation, Methodology, Validation, Visualization, Writing – original draft. **Tarek L. Rashwan:** Funding acquisition, Visualization, Writing – review & editing. **Jason I. Gerhard:** Conceptualization, Funding acquisition, Methodology, Project administration, Resources, Supervision, Writing – review & editing.

Acknowledgements

The authors would like to acknowledge Kia Barrow and Reagan Campbell for their contributions to setting-up and monitoring smouldering experiments as well as their help refining the GC-TCD methodology. We would also like to thank Dr. Gavin Grant and Dr. Dave Major for initially bringing perplexing emissions data to us, which eventually became the catalyst for this study. We dedicate this paper in loving memory to our colleague, mentor, and dear friend, Dr. Jason Ian Gerhard.

Appendix A. Supplementary data

Supplementary data to this article can be found online at https://doi.org/10.1016/j.ijhydene.2024.05.289.

References

[1] U.S. EIA, Nalley S, LaRose A. International Energy Outlook 2021, 2021.
[2] IPCC, Masson-Delmotte PZV, Pirani A, Connors SL, Péan C, Berger S, Caud N, Chen Y, Goldfarb L, Gomis MI, Huang M, Leitzell K, Lonnoy E, Matthews JBR, Maycock TK, Waterfield T, Yelekçi O, Yu R, Zhou B. Summary for Policymakers, climate change 2021: the Physical science basis. Contribution of working Group I to the sixth assessment report of the intergovernmental panel on climate change. 2021.
[3] Guo J, Kubli D, Saner P. The economics of climate change: no action not an option. 2021.
[4] REN21, Renewables 2021. Global status report. 2021.
[5] Clark WW, Rifkin J. A green hydrogen economy. Energy Pol 2006;34:2630–9. https://doi.org/10.1016/j.enpol.2005.06.024.
[6] Muradov NZ, Veziroğlu TN. From hydrocarbon to hydrogen-carbon to hydrogen economy. Int J Hydrogen Energy 2005;30:225–37. https://doi.org/10.1016/j.ijhydene.2004.03.033.
[7] Muradov NZ, Veziroğlu TN. "Green" path from fossil-based to hydrogen economy: an overview of carbon-neutral technologies. Int J Hydrogen Energy 2008;33:6804–39. https://doi.org/10.1016/j.ijhydene.2008.08.054.
[8] Pudukudy M, Yaakob Z, Mohammad M, Narayanan B, Sopian K. Renewable hydrogen economy in Asia - opportunities and challenges: an overview. Renew Sustain Energy Rev 2014;30:743–57. https://doi.org/10.1016/j.rser.2013.11.015.
[9] IEA. Global hydrogen review 2023. 2023. www.iea.org.
[10] Shiva Kumar S, Himabindu V. Hydrogen production by PEM water electrolysis – a review. Mater Sci Energy Technol 2019;2:442–54. https://doi.org/10.1016/j.mset.2019.03.002.
[11] Basile A, Liguori S, Iulianelli A. Membrane reactors for methane steam reforming (MSR). Membrane Reactors for Energy Applications and Basic Chemical Production 2015:31–59. https://doi.org/10.1016/B978-1-78242-223-5.00002-9.

[12] Sayer M, Ajanovic A, Haas R. Economic and environmental assessment of different hydrogen production and transportation modes. Int J Hydrogen Energy 2024;65:626–38. https://doi.org/10.1016/j.ijhydene.2024.04.073.
[13] Ajanovic A, Sayer M, Haas R. The economics and the environmental benignity of different colors of hydrogen. Int J Hydrogen Energy 2022;47:24136–54. https://doi.org/10.1016/j.ijhydene.2022.02.094.
[14] Halder P, Babaie M, Salek F, Haque N, Savage R, Stevanovic S, Bodisco TA, Zare A. Advancements in hydrogen production, storage, distribution and refuelling for a sustainable transport sector: hydrogen fuel cell vehicles. Int J Hydrogen Energy 2024;52:973–1004. https://doi.org/10.1016/j.ijhydene.2023.07.204.
[15] Nemitallah MA, Alnazha AA, Ahmed U, El-Adawy M, Habib MA. Review on techno-economics of hydrogen production using current and emerging processes: status and perspectives. Results in Engineering 2024;21. https://doi.org/10.1016/j.rineng.2024.101890.
[16] Noussan M, Raimondi PP, Scita R, Hafner M. The role of green and blue hydrogen in the energy transition—a technological and geopolitical perspective. Sustainability 2021;13:1–26. https://doi.org/10.3390/su13010298.
[17] Scott K. Chapter 1 introduction to electrolysis, electolysers and hydrogen production. Royal Society of Chemistry; 2019. https://doi.org/10.1039/9781788016049-00001.
[18] Revankar ST. Nuclear hydrogen production. In: Storage and hybridization of nuclear energy: techno-economic integration of renewable and nuclear energy. Elsevier; 2018. p. 49–117. https://doi.org/10.1016/B978-0-12-813975-2.00004-1.
[19] Ahmad AA, Zawawi NA, Kasim FH, Inayat A, Khasri A. Assessing the gasification performance of biomass: a review on biomass gasification process conditions, optimization and economic evaluation. Renew Sustain Energy Rev 2016;53:1333–47. https://doi.org/10.1016/j.rser.2015.09.030.
[20] Heidenreich S, Foscolo PU. New concepts in biomass gasification. Prog Energy Combust Sci 2015;46:72–95. https://doi.org/10.1016/j.pecs.2014.06.002.
[21] Lu X, Cao L, Wang H, Peng W, Xing J, Wang S, Cai S, Shen B, Yang Q, Nielsen CP, McElroy MB. Gasification of coal and biomass as a net carbon-negative power source for environment-friendly electricity generation in China. Proc Natl Acad Sci U S A 2019;116:8206–13. https://doi.org/10.1073/pnas.1812239116.
[22] Cao L, Yu IKM, Xiong X, Tsang DCW, Zhang S, Clark JH, Hu C, Ng YH, Shang J, Ok YS. Biorenewable hydrogen production through biomass gasification: A review and future prospects. Environ Res 2020;186:109547. https://doi.org/10.1016/j.envres.2020.109547.
[23] Vittoria Benedetti FPMB. Characterization of char from biomass gasification and its similarities with activated carbon in adsorption applications. Appl Energy 2018;227:92–9.
[24] Kuo PC, Illathukandy B, Wu W, Chang JS. Energy, exergy, and environmental analyses of renewable hydrogen production through plasma gasification of microalgal biomass. Energy 2021;223. https://doi.org/10.1016/j.energy.2021.120025.
[25] Switzer C, Gerhard JI, Pironi P, Rein G, Torero JL. Self-sustaining smouldering combustion: a novel remediation process for non-aqueous phase liquids in porous media. Environ Sci Technol 2009;43:5871–7. https://doi.org/10.1021/es803483s.
[26] Pironi P, Switzer C, Gerhard JI, Rein G, Torero JL. Self-sustaining smoldering combustion for NAPL remediation: laboratory evaluation of process sensitivity to key parameters. Environ Sci Technol 2011;45:2980–6. https://doi.org/10.1021/es102969z.
[27] Grant GP, Major DW, Scholes GC, Horst J, Hill S, Klemmer MR, Couch JN. Smouldering combustion (STAR) for the treatment of contaminated soils: examining limitations and defining success. Remediation 2016;26:27–51. https://doi.org/10.1002/rem.
[28] Scholes GC, Gerhard JI, Grant GP, Major DW, Vidumsky JE, Switzer C, Torero JL. Smoldering remediation of coal-tar-contaminated soil: pilot field tests of STAR. Environ Sci Technol 2015;49:14334–42. https://doi.org/10.1021/acs.est.5b03177.
[29] Sabadell G, Scholes G, Thomas D, Murray C, Bireta P, Grant G, Major D. EX situ treatment of organic wastes or oil-impacted soil using a smoldering process, vol. 231; 2019. p. 367–76. https://doi.org/10.2495/WM180341.
[30] Rashwan TL, Gerhard JI, Grant GP. Application of self-sustaining smouldering combustion for the destruction of wastewater biosolids. Waste Management 2016;50:201–12. https://doi.org/10.1016/j.wasman.2016.01.037.
[31] Duchesne AL, Brown JK, Patch DJ, Major D, Weber KP, Gerhard JI. Remediation of PFAS-contaminated soil and granular activated carbon by smoldering combustion. Environ Sci Technol 2020;54:12631–40. https://doi.org/10.1021/acs.est.0c03058.
[32] Ohlemiller TJ. Modeling of smoldering combustion propagation. Prog Energy Combust Sci 1985;11:277–310.
[33] Torero JL, Gerhard JI, Martins MF, Zanoni MAB, Rashwan TL, Brown JK. Processes defining smouldering combustion: integrated review and synthesis. Prog Energy Combust Sci 2020;81:1–48.
[34] Zanoni MAB, Torero JL, Gerhard JI. Delineating and explaining the limits of self-sustained smouldering combustion. Combust Flame 2019;201:78–92. https://doi.org/10.1016/j.combustflame.2018.12.004.
[35] Yerman L, Hadden RM, Carrascal J, Fabris I, Cormier D, Torero JL, Gerhard JI, Krajcovic M, Pironi P, Cheng YL. Smouldering combustion as a treatment technology for faeces: exploring the parameter space. Fuel 2015;147:108–16. https://doi.org/10.1016/j.fuel.2015.01.055.
[36] Ohlemiller TJ, Lucca DA. An experimental comparison of forward and reverse smolder propagation in permeable fuel beds. Combust Flame 1983;54:131–47. https://doi.org/10.1016/0010-2180(83)90027-5.
[37] Wang J, Grant GP, Gerhard JI. The influence of porous media heterogeneity on smouldering remediation. J Contam Hydrol 2021;237. https://doi.org/10.1016/j.jconhyd.2020.103756.
[38] Serrano A, Wyn H, Dupont L, Villa-Gomez DK, Yermán L. Self-sustaining treatment as a novel alternative for the stabilization of anaerobic digestate. J Environ Manage 2020;264. https://doi.org/10.1016/j.jenvman.2020.110544.
[39] Monhol FAF, Martins MF. Cocurrent combustion of human feces and polyethylene waste. Waste Biomass Valorization 2015;6:425–32. https://doi.org/10.1007/s12649-015-9359-2.
[40] Rashwan TL, Fournie T, Green M, Duchesne AL, Brown JK, Grant GP, Torero JL, Gerhard JI. Applied smouldering for co-waste management: benefits and trade-offs. Fuel Process Technol 2023;240. https://doi.org/10.1016/j.fuproc.2022.107542.
[41] Baud G, Salvador S, Debenest G, Thovert JF. New granular model medium to investigate smoldering fronts propagation-experiments. Energy Fuel 2015;29:6780–92. https://doi.org/10.1021/acs.energyfuels.5b01325.
[42] Martins MF, Salvador S, Thovert JF, Debenest G. Co-current combustion of oil shale - Part 2: structure of the combustion front. Fuel 2010;89:133–43. https://doi.org/10.1016/j.fuel.2009.06.040.
[43] Acharya B, Dutta A, Basu P. Chemical-looping gasification of biomass for hydrogen-enriched gas. Energy Fuel 2009;23:5077–83. https://doi.org/10.1021/ef9003889.
[44] Han L, Wang Q, Yang Y, Yu C, Fang M, Luo Z. Hydrogen production via CaO sorption enhanced anaerobic gasification of sawdust in a bubbling fluidized bed. Int J Hydrogen Energy 2011;36:4820–9. https://doi.org/10.1016/j.ijhydene.2010.12.086.
[45] Pfeifer C, Puchner B, Hofbauer H. Comparison of dual fluidized bed steam gasification of biomass with and without selective transport of CO2. Chem Eng Sci 2009;64:5073–83. https://doi.org/10.1016/j.ces.2009.08.014.
[46] Speight JG. Synthesis gas and the fischer–tropsch process, the refinery of the future. 2020. p. 427–68. https://doi.org/10.1016/B978-0-12-816994-0.00012-9.
[47] Guoxin H, Hao H. Hydrogen rich fuel gas production by gasification of wet biomass using a CO2 sorbent. Biomass Bioenergy 2009;33:899–906. https://doi.org/10.1016/j.biombioe.2009.02.006.
[48] Criado YA, Alonso M, Abanades JC. Kinetics of the CaO/Ca(OH)2 hydration/dehydration reaction for thermochemical energy storage applications. Ind Eng Chem Res 2014;53:12594–601. https://doi.org/10.1021/ie404246p.
[49] Irabien A, Viguri JR, Ortiz I. Thermal dehydration of calcium hydroxide. 1. Kinetic model and parameters. Ind Eng Chem Res 1990;29:1599–606. https://doi.org/10.1021/ie00104a004.
[50] Miry SZ, Zanoni MAB, Rashwan TL, Torero JL, Gerhard JI. Investigation of multi-dimensional transfer effects in applied smouldering systems: a 2D numerical modelling approach. Combust Flame 2022;246:112385. https://doi.org/10.1016/J.COMBUSTFLAME.2022.112385.
[51] Zanoni MAB, Wang J, Gerhard JI. Understanding pressure changes in smouldering thermal porous media reactors. Chem Eng J 2021;412:128642. https://doi.org/10.1016/J.CEJ.2021.128642.
[52] Rashwan TL, Torero JL, Gerhard JI. Heat losses in a smouldering system: the key role of non-uniform air flux. Combust Flame 2021;227:309–21. https://doi.org/10.1016/j.combustflame.2020.12.050.
[53] Rashwan TL, Gerhard JI, Grant GP. Application of self-sustaining smouldering combustion for the destruction of wastewater biosolids, vol. 50; 2016. p. 201–12.
[54] Rashwan TL, Zanoni MAB, Wang J, Torero JL, Gerhard JI. Elucidating the characteristic energy balance evolution in applied smouldering systems. Energy 2023;273. https://doi.org/10.1016/j.energy.2023.127245.
[55] Zanoni MAB, Torero JL, Gerhard JI. Determining the conditions that lead to self-sustained smouldering combustion by means of numerical modelling. Proc Combust Inst 2019;37:4043–51. https://doi.org/10.1016/J.PROCI.2018.07.108.
[56] Fabris I, Cormier D, Gerhard JI, Bartczak T, Kortschot M, Torero JL, Cheng YL. Continuous, self-sustaining smouldering destruction of simulated faeces. Fuel 2017;190:58–66. https://doi.org/10.1016/j.fuel.2016.11.014.
[57] Kinsman L, Torero JL, Gerhard JI. Organic liquid mobility induced by smoldering remediation. J Hazard Mater 2017;325:101–12. https://doi.org/10.1016/j.jhazmat.2016.11.049.
[58] Li J, Yin Y, Zhang X, Liu J, Yan R. Hydrogen-rich gas production by steam gasification of palm oil wastes over supported tri-metallic catalyst. Int J Hydrogen Energy 2009;34:9108–15. https://doi.org/10.1016/j.ijhydene.2009.09.030.
[59] Chang ACC, Chang HF, Lin FJ, Lin KH, Chen CH. Biomass gasification for hydrogen production. In: Int J hydrogen energy; 2011. p. 14252–60. https://doi.org/10.1016/j.ijhydene.2011.05.105.
[60] Zhang Y, Xu P, Liang S, Liu B, Shuai Y, Li B. Exergy analysis of hydrogen production from steam gasification of biomass: a review. Int J Hydrogen Energy 2019;44:14290–302. https://doi.org/10.1016/j.ijhydene.2019.02.064.